The following publication Y. Yang, S. Tan and S. Y. R. Hui, "Mitigating Distribution Power Loss of DC Microgrids With DC Electric Springs," in IEEE Transactions on Smart Grid, vol. 9, no. 6, pp. 5897-5906, Nov. 2018 is available at https://doi.org/10.1109/TSG.2017.2698578.

Mitigating Distribution Power Loss of DC Microgrids with DC Electric Springs

Yun Yang, *Student Member, IEEE*, Siew-Chong Tan, *Senior Member, IEEE* and Shu Yuen Ron Hui, *Fellow, IEEE*

***Abstract*--DC microgrids fed with substantial intermittent renewable energy sources (RES) face the immediate problem of power imbalance and the subsequent DC bus voltage fluctuation problem (that can easily breach power system standards). It has recently been demonstrated that DC electric springs (DCES), when connected with series non-critical loads, are capable of stabilizing the voltage of local nodes and improving the power quality of DC microgrids without large energy storage. In this paper, two centralized model predictive control (CMPC) schemes with (i) non-adaptive weighting factors and (ii) adaptive weighting factors are proposed to extend the existing functions of the DCES in the microgrid. The control schemes coordinate the DCES to mitigate the distribution power loss in the DC microgrids, while simultaneously providing their original function of DC bus voltage regulation. Using the DCES model that was previously validated with experiments, simulations based on MATLAB/SIMULINK platform are conducted to validate the control schemes. The results show that with the proposed CMPC schemes, the DCES are capable of eliminating the bus voltage offsets as well as reducing the distribution power loss of the DC microgrid.**

***Index Terms*--DC microgrids, DC electric springs (DCES), centralized model predictive control (CMPC), non-adaptive weighting factors, adaptive weighting factors, distribution power loss.**

I. Introduction

DC microgrids are gaining increasing attention in the microgrid community due to various merits such as high reliability, high efficiency and ease of renewable energy source (RES) interconnection, as compared to AC microgrids [1]−[6]. Many microgrid facilities such as fuel cells, photovoltaic (PV) systems, battery systems, and electronics loads such as computers and TVs are inherently of DC nature. Therefore, the normal front-end AC/DC conversion stage and its associated hardware infrastructures can be eliminated in the DC microgrids. This significantly improves the reliability and efficiency of the energy transmission [7]. However, similar to their AC counterparts, DC microgrids also suffer from significant bus voltage fluctuations induced by the RES, especially the DC voltage offsets, if the energy storage capacities are insufficient. Additionally, the instantaneous power imbalance between the power generation and the power consumption can lead to severe instability of the DC microgrids that may cause catastrophic blackouts. Therefore, well designed regulation schemes to stabilize the bus voltage of the DC microgrids are critical for the grid connections of those voltage sensitive loads.

DC electric spring (DCES), which originates from the concept of AC electric spring (ES) [8], is one of the schemes to stabilize and improve the power quality of DC microgrids [9], [10]. Being analogous to the ES in the AC microgrids, DCES are associated with non-critical loads to function as a new type of smart loads. The named non-critical loads refer to those appliances that can tolerate a wide range of voltage and power fluctuation. So far, several versions of AC ES-based smart loads are validated to improve the regulations of microgrids with grid voltage regulation [8], [11]−[16], energy storage reduction [17], power factor correction [18], neutral current minimization [19], three-phase power balance [20], and frequency stabilization [16], [21]. The first version of ES (ES-I) in [8] is limited to compensate the reactive power of the grids, since energy storage components are not included. For this reason, the second version of ES (ES-II) comprising batteries is later proposed to achieve both active and reactive power compensation [14].

The DCES follows the general configuration of ES-II. It has been investigated for the functions of bus-voltage stabilization, fault ride-through, and harmonics reduction [9], [10], [22], [23]. In [9], DCES are proved to effectively stabilize the bus voltage with unstable supply voltage of RES and alleviate the droop effect along a radical DC network for both constant-resistive and constant-power loads as non-critical loads. In [10], DCES are extended from the traditional series-type DCES (which is connected in series with the non-critical load) to the shunt-type DCES (which is connected in parallel with the non-critical load). Similar to the low power battery system [24], [25], the shunt-type DCES has a faster dynamic performance than the series-type DCES. Besides, the shunt-type DCES can reduce the harmonics of the bus voltage with less energy consumption than the series-type DCES. However, [10] also points out that series-type DCES has less energy storage capacities as compared to the shunt-type DCES, since the power consumption of the non-critical load can be manipulated by the control of DCES. Meanwhile, both series-type and shunt-type DCES are verified to eliminate the double-line frequency harmonics and support the fault-ride-through of the DC microgrid. Except [10], most of the published papers on DCES are based on the series-type DCES. In [22], the photovoltaic (PV) system is incorporated into the DCES to replace the battery systems in order to reduce energy storage capacities. Reference [23] extends the topologies of DCES from bi-directional full bridge inverters to bi-directional paralleled

Manuscript received January 9, 2017; revised February 24, 2017; accepted April 24, 2017. This work is supported by the Hong Kong Research Grant Council under Theme-based Research Project: T23-701/14-N.

Y. Yang and S. C. Tan are with the Department of Electrical and Electronic Engineering, The University of Hong Kong, Hong Kong (e-mail: yangyun@eee.hku.hk, sctan@eee.hku.hk).

S. Y. R. Hui is with the Department of Electrical and Electronic Engineering, The University of Hong Kong, Hong Kong and also with the Department of Electrical and Electronic Engineering, Imperial College London, London SW7 2AZ, U.K. (e-mail: ronhui@eee.hku.hk).

buck-boost converters and bi-directional phase-shift full-bridge converters.

Research reported on the use of DCES primarily focuses on the use of single unit. Coordinated use of multiple DCES has not been explored. In view of this, the use of multiple DCES involving a new centralized controller is presented in this paper. This controller is a high-level centralized model predictive controller (CMPC) that generates the required voltage references for the different DCES located on various buses of the microgrid. The local proportional-integral (PI) controllers of the respective DCES will be operated to track these voltage references to achieve the overall required functions. Model predictive control (MPC) is a well-known process control strategy of which future control inputs and system response are predicted using a model and are optimized at regular intervals with respect to a performance index [26]. MPC inherits several advantages. First, the underlying idea of MPC is intuitive and does not involve complicated plant modeling. Second, the basic formulation of MPC is easily extendable to different multivariable plants with almost no modification. Third, the control objectives of MPC can be readily reconfigured by changing the cost function. Fourth, MPC can deal routinely with equipment and safety constraints [27].

By incorporating the terms of distribution power loss and bus voltage deviations into the feedback, this project shows that the CMPC can enhance the operation of the DCES in terms of reducing the distribution loss in the DC microgrids. This is possible since practical loads, even for the critical loads, can tolerate a certain degree of voltage offset. The benefits of allowing the bus voltage to deviate within an acceptable percentage are to reconfigure the power flow paths of the microgrid to reduce the power loss on the distribution lines. This is achieved by manipulating the weighting factors of the cost function and executing the algorithm of CMPC to minimize the cost function. Certainly, the constraints of the bus voltage have to be included in the algorithm to guarantee the safe operation of the entire DC microgrid. For the weighting factors design, the operations of the CMPC with both non-adaptive and adaptive weighting factors are presented and compared. This comparative study is based on computer simulations using a DCES model that has previously been verified with experiments [9], [10]. Compared with the droop control strategies reported in [28] and [29], the proposed CMPC is built upon the local control strategy of DCES, making it more suitable for small-scale DC microgrids.

II. Equivalent Model and Local Control of DCES

A simplified DC microgrid consists of n RES units and m buses is shown in Fig. 1 [30]. The loads on each bus can be classified as non-critical loads (NL) and critical loads (CL) [8]. NL are loads that can tolerate a relatively large degree of power and voltage fluctuations. Examples are thermal loads such as water heaters, heat pumps and thermal storage systems. CL are voltage sensitive loads that require well-regulated bus voltage, such as medical equipment. Generally, the NL are resistive loads and the CL can be resistive loads or constant power loads. The RES can be wind energy sources, solar energy sources and biofuel energy sources. The intermittency and uncertainty of these RES give rise to the difficulty in achieving instantaneous power balance between the supply side and the demand side. To overcome this problem, battery systems are typically installed to buffer the instantaneous power imbalance and stabilize the bus voltage. However, this battery solution is expensive and has limited energy capacities [31]. The distributed smart loads (SL) based on DC electric springs (DCES) involves simple power electronics and thus provide a competitive means of achieving distributed power compensation [9], [10], [22], [23] with the possibility of reducing energy storage requirements.

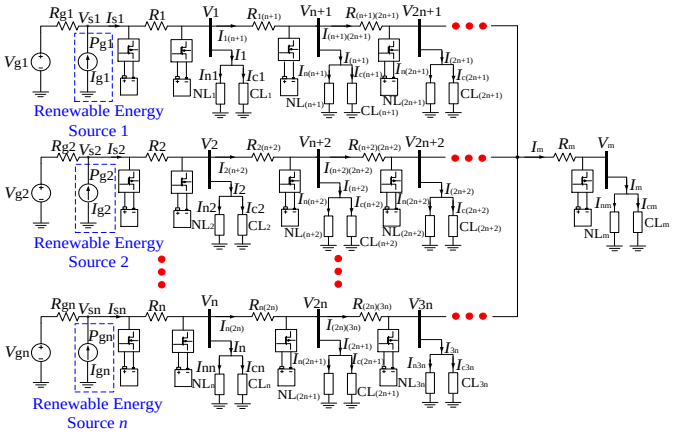

Fig. 1. An m-bus DC microgrid with n RES units.

A simplified diagram of a DCES installed at one of the DC microgrid buses is shown in Fig. 2. The DCES is connected to the non-critical load R_n in series to form a smart load. Here, V_g is a constant voltage source, indicating the traditional DC power supply; R_g is the internal resistance of V_g; I_R is a time-varying current source, indicating the RES supply; R_d is the resistive distribution line; R_c is the critical load; V_n is the voltage over the non-critical load; V_{ES} is the ES voltage; and V_{bus} is the bus voltage. The equivalent circuit of the system in Fig. 2 is shown in Fig. 3(a), which is a newly proposed model that has not been reported in previous works. Without DCES, if the power supply side and the demand side are balanced, the nominal power P_{nom} can be derived as

$$P_{\text{nom}} = V_{\text{nom}}^2 \frac{R_n + R_c}{R_n R_c}, \tag{1}$$

where V_{nom} is the nominal bus voltage.

However, the actual power of the bus P can be different from the nominal power P_{nom} as

$$P = V_{\text{bus}}^2 \frac{R_n + R_c}{R_n R_c}. \tag{2}$$

Then, the difference between the nominal and the actual power of the bus is

$$\Delta P = P_{\text{nom}} - P. \tag{3}$$

Substituting (1) and (2) into (3),

$$\Delta P = \left(V_{\text{nom}} - V_{\text{bus}}\right)\left(V_{\text{nom}} + V_{\text{bus}}\right)\frac{R_n + R_c}{R_n R_c}. \tag{4}$$

According to (4), when the power supply is insufficient, $\Delta P>0$ and the bus voltage $V_{bus}<V_{nom}$. When the power supply is excessive, $\Delta P<0$ and the bus voltage $V_{bus}>V_{nom}$. When the power supply and demand are balanced, $\Delta P=0$, the bus voltage $V_{bus}=V_{nom}$. As to the RES, the power supply often fluctuates, so ΔP is unsteady and so V_{bus} varies with offsets.

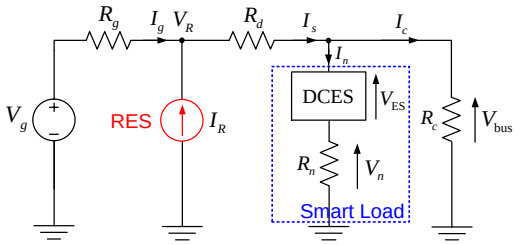

Fig. 2. Simplified diagram of a DC microgrid bus with a DCES.

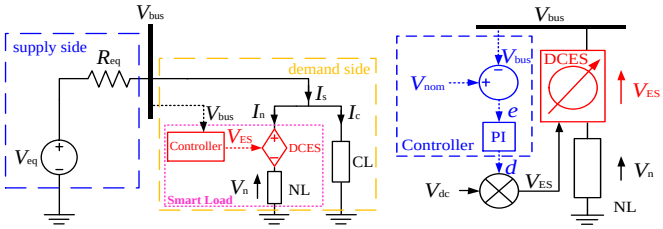

(a) Simplified topology (b) Local control strategy

Fig. 3. Equivalent model of a DC microgrid bus with a DCES.

However, when the DCES is installed,

$$V_{\text{bus}} = \left(\frac{P}{V_{\text{bus}}} - \frac{V_n}{R_n} \right) R_c = V_{\text{ES}} + V_n , \tag{5}$$

Re-arranging V_{ES} as the subject of the equation,

$$V_{\text{ES}} = \frac{R_n + R_c}{R_c} V_{\text{bus}} - \frac{PR_n}{V_{\text{bus}}} . \tag{6}$$

Hence, only if V_{ES} is regulated at

$$V_{\text{ES}} = \frac{R_n + R_c}{R_c} V_{\text{nom}} - \frac{PR_n}{V_{\text{nom}}} , \tag{7}$$

the bus voltage will be equal to the nominal bus voltage, i.e., $V_{\text{bus}}=V_{\text{nom}}$. The V_{ES}–P curve can be depicted as shown in Fig. 4, where V_{ESmax} and V_{ESmin} are the maximum and minimum voltage DCES, respectively. Obviously, when the power supply is insufficient such that $P<P_{\text{nom}}$, the DCES is activated as a voltage source within the range of $0<V_{\text{ES}}\le V_{\text{ESmax}}$. When the power supply is excessive such that $P>P_{\text{nom}}$, the DCES is activated as a voltage sink within the range of $V_{\text{ESmin}}\le V_{\text{ES}}<0$. When the power is balanced such that $P=P_{\text{nom}}$, the DCES is deactivated as $V_{\text{ES}}=0$.

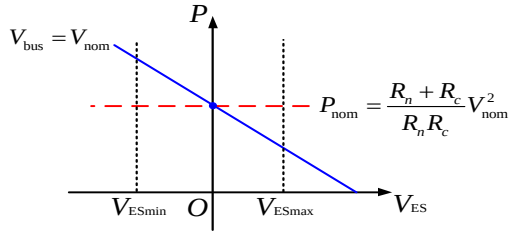

Fig. 4. V_{ES}–P curve.

The local control strategy of DCES is given in Fig. 3(b). A classic PI controller is used to regulate the bus voltage. The corresponding control block diagram in the frequency domain is shown in Fig. 5.

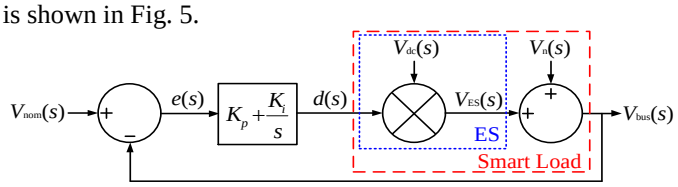

Fig. 5. Control block diagram of the classic local control strategy for DCES.

The closed-loop transfer function of the system is

$$\frac{V_{\text{bus}}(s)}{V_{\text{nom}}(s)} = \frac{K_p V_{\text{dc}} s + K_i V_{\text{dc}}}{\left(1 + K_p V_{\text{dc}}\right) s + K_i V_{\text{dc}}} . \tag{8}$$

The transfer function between the error signal $e(s)$ and the reference signal $V_{\text{nom}}(s)$ is

$$\frac{e(s)}{V_{\text{nom}}(s)} = \frac{V_{\text{nom}}(s) - V_{\text{bus}}(s)}{V_{\text{nom}}(s)} = \frac{s}{\left(1 + K_p V_{\text{dc}}\right) s + K_i V_{\text{dc}}} . \tag{9}$$

Then, the steady-state error for a unit-step response can be obtained by applying the final-value theorem as

$$e_{\text{ss}} = \lim_{s \to 0} s e(s) = 0 , \tag{10}$$

which means the bus voltage V_{bus} can track the reference V_{nom}. from 0 V to 8.5 V.

III. Centralized Model Predictive Control of DCES

For an m-bus DC microgrid, a maximum of $m(m\text{-}1)/2$ distribution lines can be possibly installed to link any two of the buses. However, the actual number of distribution lines is less than $m(m\text{-}1)/2$, since some of the buses are not connected. For instance, the DC microgrid in Fig. 1 has $3(m\text{-}1)/n$ distribution lines, which is less than $m(m\text{-}1)/2$. Hence, the state of the connections between any two buses is denoted as $C_{ij} \in \{0,1\}$, where C_{ij} =1 indicates the bus i and the bus j are connected and C_{ij} =0 indicates the bus i and the bus j are disconnected. Besides, the resistance of the distribution line between the bus i and the bus j is denoted as R_{ij}; The voltage of the bus i is denoted as V_{busi}; The total power supplied by the sources is denoted as P_{s}; The total power stored or supplied by the batteries is denoted as P_{b}; The total power consumed by the constant power loads is denoted as P_{pl}; The resistance of the critical load at the bus i is denoted as R_{ci}; The resistance of the non-critical load at the bus i is denoted as R_{ni};

For an m-bus DC microgrid, the power supply and demand are balanced if

$$P_{\text{s}} - \sum_{i=1}^{m-1} \left[\sum_{j=i+1}^{m} C_{ij} \frac{\left(V_{busi} - V_{busj}\right)^2}{R_{ij}} \right] = P_{\text{b}} + P_{\text{pl}} + \sum_{i=1}^{m} V_{busi}^2 \left(\frac{R_{ni} + R_{ci}}{R_{ni} R_{ci}} \right) , \tag{11}$$

where $P_{\text{b}}>0$ indicates the batteries absorbing excessive power and $P_{\text{b}}<0$ indicates the batteries providing insufficient power. However, when the RES extract more power significantly than the nominal power, the power supply and demand are not balanced even if the batteries operate at the maximum capacity

$$\begin{aligned} \Delta P = \Delta P_{\text{s}} - \left(P_{\text{bmax}} - P_{\text{b}} \right) = \sum_{i=1}^{m} \left(V'^2_{busi} - V^2_{busi} \right) \left(\frac{R_{ni} + R_{ci}}{R_{ni} R_{ci}} \right) \\ + \sum_{i=1}^{m-1} \left[\sum_{j=i+1}^{m} C_{ij} \frac{\left(V'_{busi} - V'_{busj}\right)^2 - \left(V_{busi} - V_{busj}\right)^2}{R_{ij}} \right] \end{aligned} , \tag{12}$$

where ΔP_{s} is the excessive source power; P_{bmax} is the maximum capacity of the batteries; ΔP is the excessive power inducing the offsets of the buses voltage; V_{busi} and V_{busj} are the nominal voltage of the bus i and the bus j, respectively; V'_{busi} and V'_{busj} are the voltage of the bus i and the bus j after the increment of the source power. Besides, according to the Thevenin's theorem, any two of the buses voltage, i.e. the bus i and the bus j in a purely resistive DC microgrid are proportional as

$$V_{busj} = kV_{busi}, \tag{13}$$

where k is positive.

Substituting (13) into (12), we have

$$\Delta P = \sum_{i=1}^{m}\left(V'_{busi} - V_{busi}\right)\left(V'_{busi} + V_{busi}\right)\left(\frac{R_{ni}+R_{ci}}{R_{ni}R_{ci}}\right) + \sum_{i=1}^{m-1}\left[\sum_{j=i+1}^{m} C_{ij}\frac{\left(V'_{busi} - V_{busi}\right)\left(V'_{busi} + V_{busi}\right)\left(1-k\right)^2}{R_{ij}}\right]. \tag{14}$$

In (14), when the RES extract more power than the nominal power such that $\Delta P>0$, $V'_{busi} > V_{busi}$ indicating the bus voltage will increase. On the contrary, when the RES extract less power than the nominal power such that $\Delta P<0$, $V'_{busi} < V_{busi}$ indicating the bus voltage will decrease.

While one DCES is effective in stabilizing a local bus voltage, multiple DCES without considering any global regulations may lead to the system instability. Such unstable phenomenon caused by multiple ES in the AC microgrid is reported in [32]. As critical loads can tolerate about 5% DC offsets, the bus voltages are allowed to have 5% offset. Therefore, the power flow of the DC microgrid can be regulated by the control of the bus voltage. Importantly, the power loss on the distribution lines can be mitigated by the global regulation of providing adequate references for the local controllers. A centralized model predictive control (CMPC) can be used as the global controller.

The objective function of the CMPC is

$$\min J = \alpha\sum_{i=1}^{m}\left(V_{nom} - V_{busi}\right)^2 + \left(1-\alpha\right)\sum_{i=1}^{m-1}\left[\sum_{j=i+1}^{m} C_{ij}\frac{\left(V_{busi} - V_{busj}\right)^2}{R_{ij}}\right] \tag{15}$$

s.t.

$$0 \le \alpha \le 1,$$

$$\left(1-\eta\right)V_{nom} \le V'_{busi} \le \left(1+\eta\right)V_{nom},$$

where V_{nom} is the nominal bus voltage of the DC microgrid; η is the voltage tolerance of the critical loads by percentage; V'_{busi} are the bus voltage with smart loads; α is the weighting factor. α = 1 means only the regulation of the bus voltage is concerned. α = 0 means only the power loss on the distribution lines is concerned. The voltage tolerance of the critical loads is generally stricter than the bus voltage tolerance. Therefore, the compliance of the constraints given in (15) will automatically guarantee the stability of the system.

The flowchart of the algorithm of the CMPC is presented in Fig. 6. Initially, the entire power loss on the distribution lines $\hat{P}_{loss}$ is predicted using the searched bus voltage and the measured bus voltage (uncertainties of the system are neglected in this work). The term $V'_{busi} = (1-\eta)V_{nom}{:}\,\Delta V'_{busi}{:}\,(1+\eta)V_{nom}$ indicates that the values of V'_{busi} are searched from $(1-\eta)V_{nom}$ to $(1+\eta)V_{nom}$ with the step of $\Delta V'_{busi}$. n denotes the number of the buses with smart loads. Then, the quadratic sums of the voltage deviations $\hat{V}_e^2$ are calculated for all the buses. By incorporating the weighting factor α, the quadratic sum of the voltage deviations $\hat{V}_e^2$ and the predicted power loss $\hat{P}_{loss}$, the objective function $J = \alpha\hat{V}_e^2 + (1-\alpha)\hat{P}_{loss}$ can be obtained to find the optimal references of the buses with smart loads. After several iterations, the optimal references of the buses with smart loads V'_{refi} are found and used for local controllers. The comprehensive control block diagram of multiple DCES in an m-bus DC microgrid is shown in Fig. 7. $V'_{busi}(k)$ $(i = 1,2,\dots,n)$ are the voltage of the buses with smart loads; $V_{busi}(k)$ $(i = n+1, n+2, \dots, m)$ are the voltage of the buses without smart loads; $u_i(k)$ $(i = 1,2,\dots,n)$ are the duty ratios of the DCES in smart loads; The sampling time k abbreviates for the sampling period of the CMPC kT_{CMPC}. It is emphasized that the sampling frequency of the CMPC f_{CMPC} is much lower than the sampling frequency of the local controllers f_{PI}, so that the local PI control can be implemented within a sampling period of the CMPC.

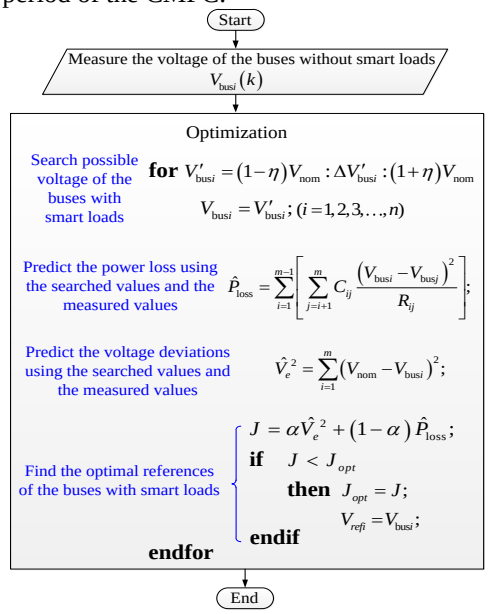

Fig. 6. Flowchart of the algorithm of the CMPC.

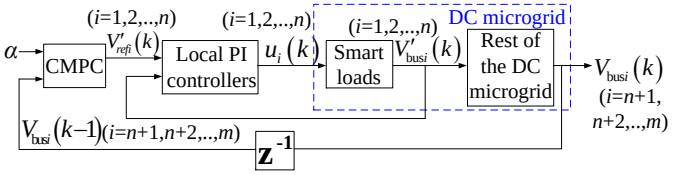

Fig. 7. Comprehensive control block diagram of multiple DCES in an m-bus DC microgrid.

The proposed CMPC can be classified as (i) CMPC with non-adaptive weighting factors and (ii) CMPC with adaptive weighting factors. The advantage of the CMPC with adaptive weighting factors over the CMPC with non-adaptive weighting factors is that the power loss on the distribution lines can be further minimized, since the weighting factor can be changed corresponding to the varying power conditions of both supply side and demand side. The flowchart of the adaptive weighting factor algorithm is shown in Fig. 8.

At the sampling time k, all the bus voltages are measured and checked. If all the bus voltages are within the tolerance, the weighting factor α decreases by a step of $\Delta\alpha$. If any one of the bus voltage is beyond the tolerance, the weighting factor α increases by a step of $\Delta\alpha$. Then, the bus voltage at the sampling time $k+\lambda$ are checked and compared with the bus voltage at the sampling time k. If any one of the bus voltage is changed, all the bus voltages are checked whether they are within the tolerance or not. If all the bus voltages are unchanged, the weighting

factor α remains unchanged. The comparison between the bus voltage at the sampling time $k+\lambda$ and the bus voltage at the sampling time k can help avoid undesirable oscillation of the bus voltage. Otherwise, the weighting factor α will decrease and increase cycle by cycle around the tolerant value even if the system power is balanced. The time sequence of the comprehensive control strategy is shown in Fig. 9.

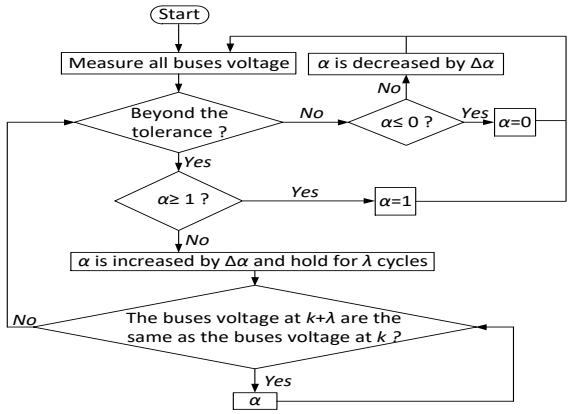

Fig. 8. Flowchart of the adaptive weighting factor algorithm.

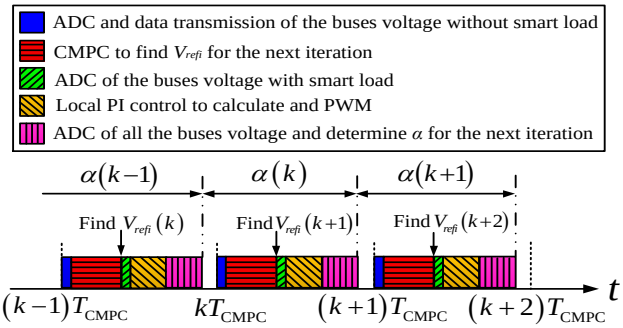

Fig. 9. Time sequence of the comprehensive control strategy.

IV. Case Study and Simulation Results

The case study is conducted on a 48 V five-bus DC microgrid without batteries. The schematic of the DC microgrid system is shown in Fig. 10. Two RES are installed at the bus 1 and the bus 5. The specifications of the DC microgrid, including the parameters of the two RES, the resistance of the distribution lines and the resistance of the loads are listed in Table I. The tolerance of the bus voltage is ±5%. i.e., 45.6 V to 50.4 V. Simulation is carried out on MATLAB/SIMULINK with the solver type of Tustin at a sampling frequency of 1 kHz.

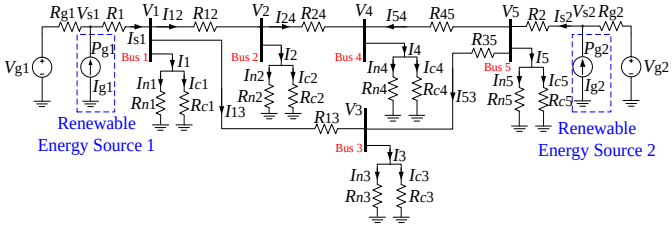

Fig. 10. A 48 V five-bus DC microgrid without batteries.

1) *DC Microgrid without DCES.*

When both RES 1 and RES 2 operate at the power rating of 624.5 W and 679.8 W, the voltages of the five buses are 49.59 V, 47.37 V, 48.12 V, 47.04 V and 49.74 V respectively, as shown in Fig. 11(b) (period 0 to 1 second). All the five bus voltages are within the ±5% tolerance. Then, P_{g1} is changed in a sequence at interviews of 1 second from 624.5 W (0% deviation of the rating power) to 1105.8 W (+77.1%) to 245.1 W (−60.8%) to 1050.2 W (+68.2%) to 346.4 W (−44.5%), and P_{g2} is changed from 679.8 W (0% deviation of the rating power) to 987.2 W (+45.2%) to 346.5 W (−49.0%) to 1170.9 W (+68.2%) to 245.2 W (−44.5%). Such changes are shown in Fig. 11(a). The waveforms of the bus voltage corresponding to the power variations of the RES are shown in Fig. 11(b). The values of the bus voltages are listed in Table II. Obviously, all the bus voltages exceed the tolerance in a certain period of time (excessive values are emphasized).

TABLE I. Specifications of the System

Description	Symbol	Value
Power rating of the RES 1	P_{g1}	11.41 kW
Internal resistance of the RES 1	R_{g1}	0.4 Ω
Internal inductance of RES 1	L_{g1}	1.07 mH
Power rating of the RES 2	P_{g2}	11.18 kW
Internal resistance of RES 2	R_{g2}	0.6 Ω
Internal inductance of RES 2	L_{g2}	1.27 mH
Impedance between bus 1 and bus 2	Z_{12}	0.3+0.0471j Ω
Impedance between bus 1 and bus 3	Z_{13}	0.2+0.0314j Ω
Impedance between bus 2 and bus 4	Z_{24}	0.1+0.0157j Ω
Impedance between bus 4 and bus 5	Z_{45}	0.4+0.0628j Ω
Impedance between bus 3 and bus 5	Z_{35}	0.3+0.0471j Ω
Non-critical load at bus 1	Z_{n1}	55 Ω
Critical load at bus 1	Z_{c1}	50 Ω
Non-critical load at bus 2	Z_{n2}	15+5.181j Ω
Critical load at bus 2	Z_{c2}	15 Ω
Non-critical load at bus 3	Z_{n3}	10–31.847j Ω
Critical load at bus 3	Z_{c3}	10 Ω
Non-critical load at bus 4	Z_{n4}	22+6.28j Ω
Critical load at bus 4	Z_{c4}	10 Ω
Non-critical load at bus 5	Z_{n5}	45 Ω
Critical load at bus 5	Z_{c5}	60 Ω

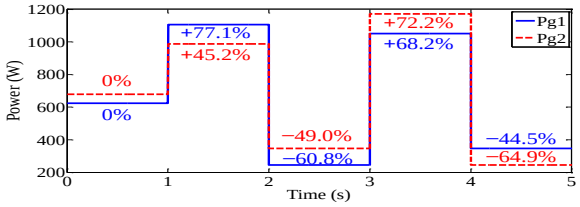

(a) Power variations of the RES

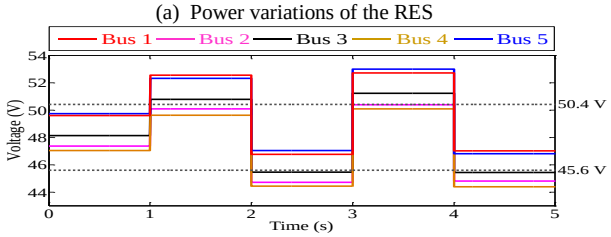

(b) Bus voltages

Fig. 11. Waveforms of the power supply by RES and the bus voltages of the DC microgrid without DCES.

TABLE II. Bus Voltages of the DC Microgrid without DCES

Bus No.	0 to 1 s	1 to 2 s	2 to 3 s	3 to 4 s	4 to 5 s
1	49.59 V	**52.54 V**	46.76 V	**52.72 V**	47.02 V
2	47.37 V	50.08 V	**44.71 V**	50.39 V	**44.81 V**
3	48.12 V	**50.77 V**	**45.45 V**	**51.22 V**	**45.42 V**
4	47.04 V	49.62 V	**44.44 V**	50.08 V	**44.39 V**
5	49.74 V	**52.31 V**	47.04 V	**53.0**	46.79

2) DC Microgrid with One DCES.

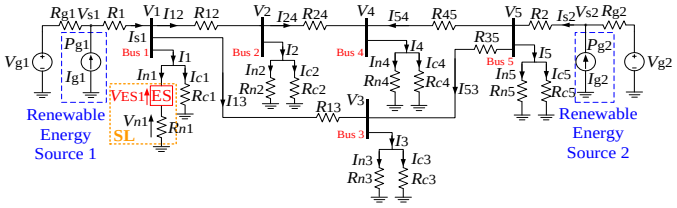

Fig. 12. The 48 V five-bus DC microgrid with one DCES installed at bus 1.

TABLE III. PARAMETERS OF THE CONTROLLERS

CMPC		Local PI controller	
Parameter	Value	Parameter	Value
Weighting factor α	1	K_p	0.05
Searching step ΔV_{bus}	0.1 V	K_i	50
Sampling frequency	1 kHz	Sampling frequency	100 kHz

Assume only one DCES is installed in the DC microgrid. Five different cases can be considered because the DCES can be installed at each of the five buses. The topology of the first case that the DCES is installed at bus 1 is shown in Fig. 12. The parameters of the CMPC and the local controller are listed in Table III. The weighting factor α of the CMPC is set to be 1, which means the precise voltage regulation is the only concern. By trial and error, the searching step of the CMPC ΔV_{bus} is set as 0.1 V. The time delay, including analogue-to-digital conversion (ADC) and the communication, is set as 0.025 ms to emulate a practical system.

Fig. 13 shows the waveforms of the bus voltages of the DC microgrid when the DCES is installed at the five buses, respectively. The values of the bus voltages in Fig. 13 are listed in Table IV.

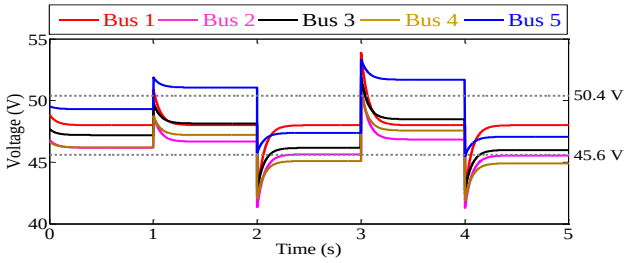

(a) At bus 1

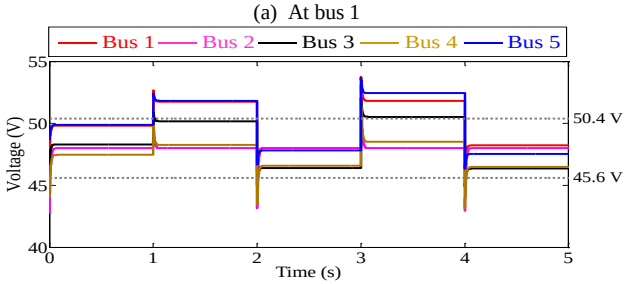

(b) At bus 2

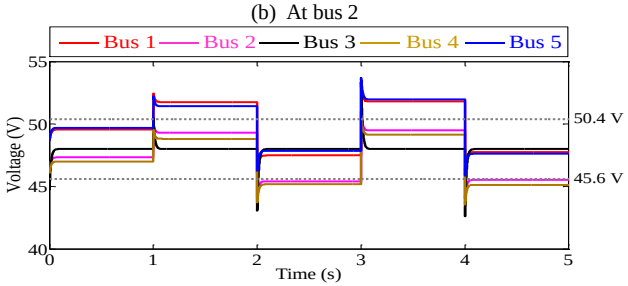

(c) At bus 3

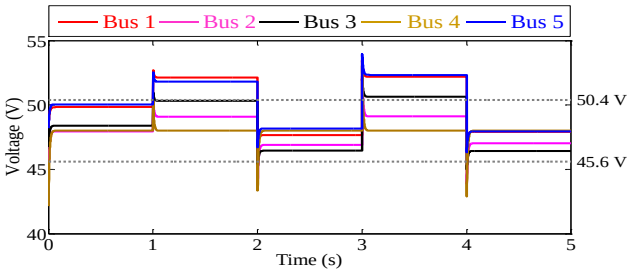

(d) At bus 4

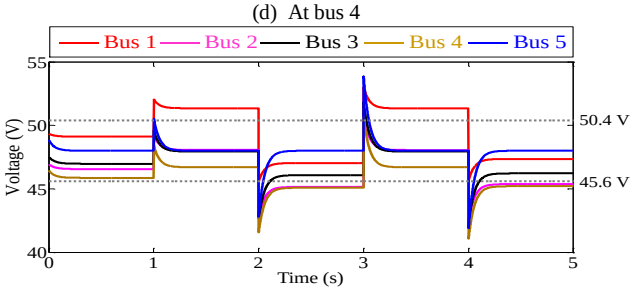

(e) At bus 5

Fig. 13. Waveforms of the bus voltages of the DC microgrid when the DCES is installed at the five buses.

TABLE IV. BUS VOLTAGES OF DC MICROGRID WITH ONE DCES

Case		0 to 1 s	1 to 2 s	2 to 3 s	3 to 4 s	4 to 5 s
ES at Bus 1	Bus 1	48.00 V	48.00 V	48.00 V	48.00 V	48.00 V
	Bus 2	46.17 V	46.67 V	45.63 V	46.84 V	**45.55 V**
	Bus 3	47.20 V	48.12 V	46.16 V	48.48 V	45.99 V
	Bus 4	46.19 V	47.20 V	**45.09 V**	47.56 V	**44.91 V**
	Bus 5	49.30 V	**51.06 V**	47.38 V	**51.69 V**	47.06 V
ES at Bus 2	Bus 1	49.83 V	**51.76 V**	48.00 V	**51.82 V**	48.22 V
	Bus 2	48.00 V	48.00 V	48.00 V	48.00 V	48.00 V
	Bus 3	48.30 V	50.17 V	46.40 V	**50.53 V**	46.35 V
	Bus 4	47.45 V	48.26 V	46.59 V	48.52 V	46.48 V
	Bus 5	49.89 V	**51.83 V**	47.81 V	**52.44 V**	47.54 V
ES at Bus 3	Bus 1	49.56 V	**51.76 V**	47.79 V	**51.81 V**	47.75 V
	Bus 2	47.34 V	49.30 V	**45.42 V**	49.48 V	**45.53 V**
	Bus 3	48.00 V	48.00 V	48.00 V	48.00 V	48.00 V
	Bus 4	47.00 V	48.82 V	**45.12 V**	49.14 V	**45.14 V**
	Bus 5	49.70 V	**51.42 V**	47.86 V	**51.96 V**	47.62 V
ES at Bus 4	Bus 1	49.83 V	**52.13 V**	47.66 V	**52.20 V**	47.93 V
	Bus 2	47.96 V	49.09 V	46.89 V	49.12 V	47.02 V
	Bus 3	48.39 V	50.32 V	46.44 V	**50.64 V**	46.43 V
	Bus 4	48.00 V	48.00 V	48.00 V	48.00 V	48.00 V
	Bus 5	50.05 V	**51.80 V**	48.17 V	**52.34 V**	47.94 V
ES at Bus 5	Bus 1	49.11 V	**51.35 V**	47.03 V	**51.33 V**	47.35 V
	Bus 2	46.56 V	48.06 V	**45.16 V**	48.05 V	**45.37 V**
	Bus 3	46.97 V	47.94 V	46.08 V	47.93 V	46.22 V
	Bus 4	45.86 V	46.70 V	**45.09 V**	46.70 V	**45.21 V**
	Bus 5	48.00 V	48.00 V	48.00 V	48.00 V	48.00 V

Clearly, the offsets of the bus voltages are mitigated for all five cases, as compared to the results in Table II. Besides, the number of the periods that the bus voltages exceeding the tolerance is significantly reduced. One index indicating the quality of the buses voltage regulation is

$$\sigma^2 = \frac{1}{N}\sum_{i=1}^{N}\left(V_{busi} - V_{nom}\right)^2, \qquad (16)$$

where N is the total number of the bus voltages, i.e., N=25 for

Table II. The comparisons of σ^2 among the DC microgrid without DCES and the DC microgrid with one DCES at the five buses are given in Fig. 14. Obviously, all the σ^2 values of the DC microgrid with one DCES are smaller than the σ^2 values of the DC microgrid without DCES. This means that even one DCES can mitigate the offsets of the bus voltages.

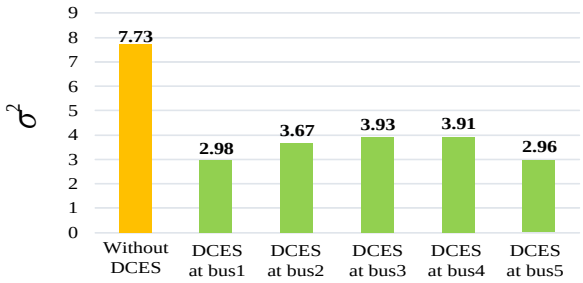

Fig. 14. Comparison of σ^2 for DC microgrid without and with one DCES.

3) DC Microgrid with Multiple DCES.

While one DCES can mitigate the offsets of the buses voltage, some of the bus voltages still exceed the tolerance. In order to make sure all the bus voltages are within the tolerance, multiple DCES are installed. Three DCES are installed at bus 1, bus 4 and bus 5, respectively. The parameters of the CMPC and local controllers are listed in Table III. With the same power variations of RES in Fig. 11(a), the buses voltage are shown in Fig. 15(a). All the five bus voltages are now within the tolerance at steady state. Furthermore, since the bus voltages are well-regulated within the tolerance, reducing the weighting factor α may reduce the power loss on the distribution lines. The waveforms of the bus voltages when α=0.9 are shown in Fig. 15(b). It can be seen that the bus voltages are still within the tolerance and the power loss on the distribution lines is reduced. The comparisons of the power loss on the distribution lines for the CMPC with α=1 and the CMPC with α=0.9 are given in Fig. 16. Integrating the difference of their power loss, the energy saving over 5 seconds is about 49.4% (the energy loss for α=1 is 1927.48 J and the energy loss for α=0.9 is 974.53 J) by only setting the weighting factor α from 1 to 0.9.

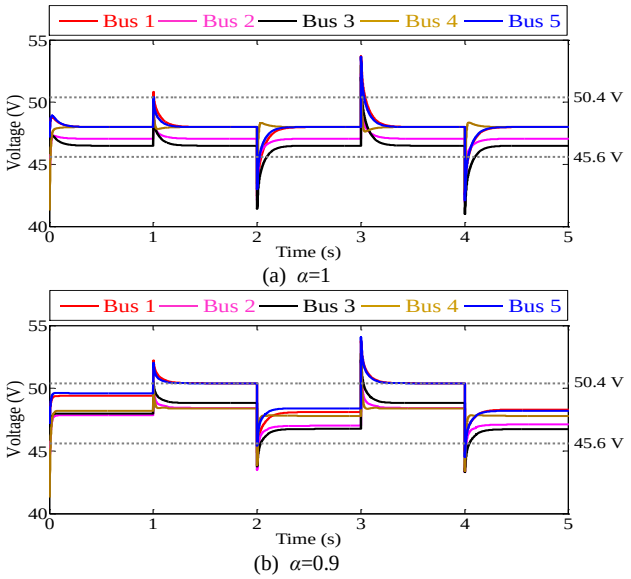

(a) α=1

(b) α=0.9

Fig. 15. Waveforms of the bus voltages of the DC microgrid with three DCES installed at bus 1, bus 4 and bus 5.

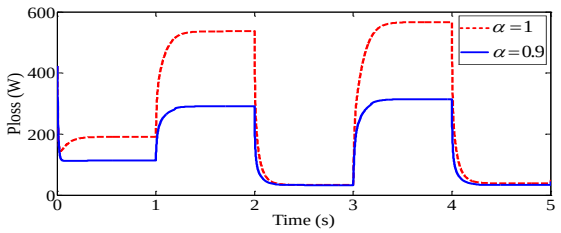

Fig. 16. The comparisons of the power loss on the distribution lines between α=1 and α=0.9 when three DCES are installed.

Next, four DCES are installed at bus 1, bus 2, bus 4, and bus 5, respectively. The searching step of the CMPC ΔV_{bus} is changed from 0.1 to 0.2 to accelerate the computing speed while the sacrifice of the searching precision is trivial. The values of the weighting factor α decrease from 1 to 0.5 with an interval of 0.1 (Note: α=0.4 results in the bus voltages exceeding the tolerance). With the same power variations of RES in Fig. 11(a), the bus voltages are shown in Fig. 17. The comparisons of the power loss on the distribution lines for the CMPC with different values of α are given in Fig. 18. These results show that the power loss on the distribution lines can be reduced significantly when α is changed from 1 to 0.9. The reduction of power loss can also be visually observed when α is changed from 0.9 to 0.8. The reduction of power loss is not distinct when α is changed from 0.8 to 0.7 to 0.6 to 0.5. Fig. 19 shows the energy saving in the 5 seconds from α=1 to 0.9, 0.8, 0.7, 0.6 and 0.5, respectively. Obviously, the most energy saving case is α=0.5.

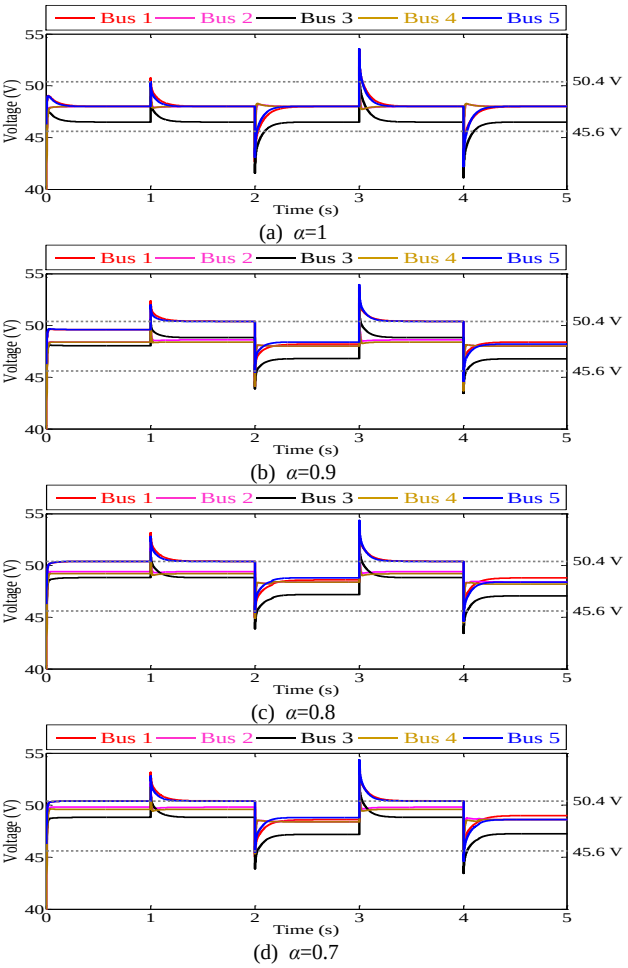

(a) α=1

(b) α=0.9

(c) α=0.8

(d) α=0.7

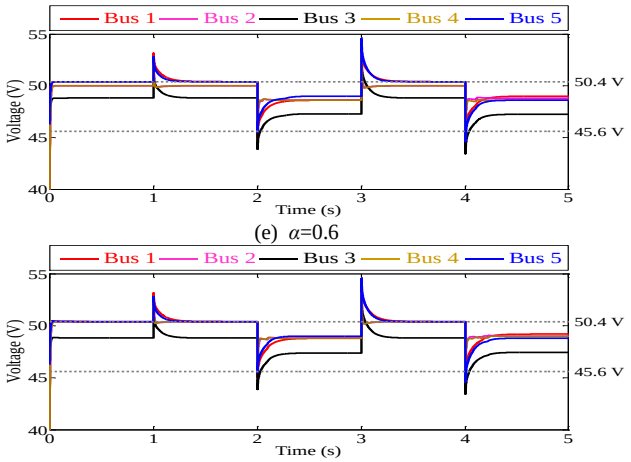

(e) α=0.6

(f) α=0.5

Fig. 17. Waveforms of the bus voltages of the DC microgrid with four DCES installed at bus 1, bus 2, bus 4 and bus 5.

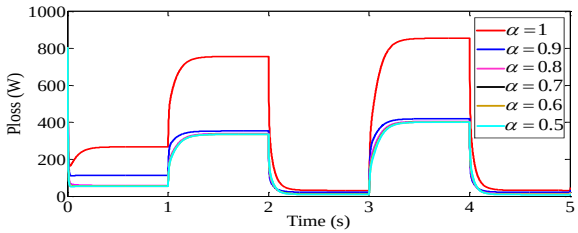

Fig. 18. Comparisons of the power loss on the distribution lines for different values of α when four DCES are installed.

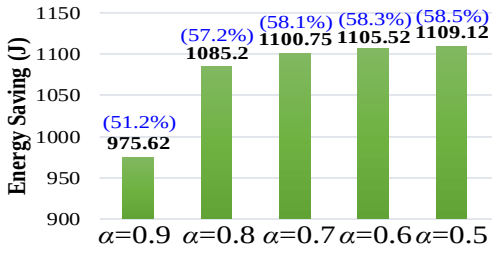

Fig. 19. Energy saving in the 5 seconds from α=1 to 0.9, 0.8, 0.7, 0.6 and 0.5.

The aforementioned CMPC refers to the CMPC with non-adaptive weighting factors. The CMPC with adaptive weighting factors can further reduce the power loss on the distribution lines. The searching step of the CMPC ΔV_{bus} is kept as 0.2 V. The parameter λ of the adaptive weighting factor algorithm in Fig. 8 is set as 5. With the same power variations of RES in Fig. 11(a), the adaptive weighting factor can change correspondingly as shown in Fig. 20. Fig. 21 shows the comparisons of the energy saving in the 5 seconds between the CMPC with non-adaptive weighting factor α=0.5 and the CMPC with adaptive weighting factor. Obviously, the CMPC with adaptive weighting factor saves about 0.8% more energy in the 5 seconds compared to the CMPC with non-adaptive weighting factor α=0.5.

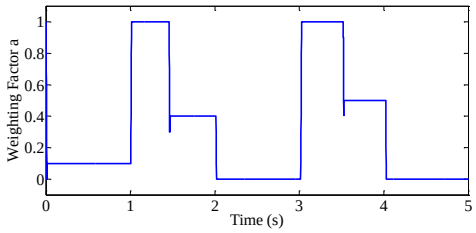

Fig. 20. Variations of the adaptive weighting factor.

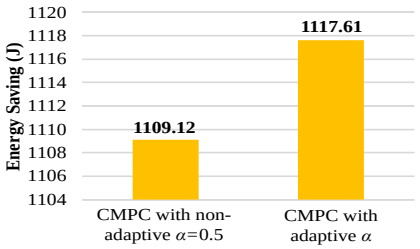

Fig. 21. Comparisons of the energy saving in the 5 seconds between the CMPC with non-adaptive weighting factor α=0.5 and the CMPC with adaptive weighting factors.

V. Conclusions

DC electric springs (DCES) is an emerging technology that can be used to stabilize and improve the power quality of DC microgrids. In this paper, a centralized model predictive control (CMPC) with both non-adaptive weighting factors and adaptive weighting factors is proposed for multiple DCES to further mitigate the power loss on the distribution lines of a DC microgrid. Using a DCES model previously verified with experiments, simulation studies have been conducted for a DC microgrid setup. Simulation results on a 48 V five-bus DC microgrid show that the energy is saved about 49.4% in the 5 seconds when three DCES are controlled by the CMPC with non-adaptive weighting factors and is saved about 58.5% in the 5 seconds when four DCES are controlled by the CMPC with non-adaptive weighting factors. It is also demonstrated that the power loss on the distribution lines of the DC microgrid can be further reduced by the CMPC with adaptive weighting factors, as compared to the CMPC with non-adaptive weighting factors.

VI. Acknowledgement

The authors would like to thank Prof. David Hill and the theme-based research project T23-701/14-N.

References

[1] B. C. Beaudreau, *World Trade: A Network Approach*, iUniverse, 2004.
[2] G. Neidhofer, "Early three-phase power," *IEEE Power and Energy Magazine*, vol. 5, no. 5, pp.88−100, Sep. 2007.
[3] R. H. Lasseter and P. Paigi, "Microgrid: a conceptual solution," in *Proc. IEEE Power Electron. Spec. Conf.*, 2004, pp. 4285−4290.
[4] S. Anand, B. Fernandes, and J. Guerrero, "Distributed control to ensure proportional load sharing and improve voltage regulation in low-voltage dc microgrids," *IEEE Tran. Pow. Elect.*, vol. 28, no. 4, Aug. 2012.
[5] T. Gragicevic, X. Lu, J. C. Vasquez, and J. M. Guerrero, "DC microgrids−part I: a review of control strategies and stabilization techniques," *IEEE Trans. Pow. Elect.*, vol. 31, no. 7, Jul. 2016.
[6] T. Gragicevic, X. Lu, J. Vasquez, and J. Guerrero, "DC microgrids−part II: a review of power architectures, applications, and standardization issues," *IEEE Trans. Power Electron.*, vol. 31, no. 5, May 2016.
[7] P. Loh, D. Li, Y. Chai, and F. Blaabjerg, "Autonomous operation of hybrid microgrid with AC and DC subgrids," *IEEE Tran. Power Electron.*, vol. 28, no. 5, pp. 2214−2223, May 2013.
[8] S. Y. R. Hui, C. K. Lee, and F. F. Wu, "Electric springs-A new smart grid technology," *IEEE Trans. Smart Grid*, vol. 3, no. 3, pp. Sep. 2012.
[9] K. T. Mok, M. H. Wang, S. C. Tan, and S. Y. R. Hui, "DC electric springs–A new technology for stabilizing DC power distribution systems," *IEEE Tran. Pow. Elect.* vol. 32, no. 2, Feb. 2017.
[10] M. H. Wang, K. T. Mok, S. C. Tan, and S. Y. R. Hui, "Multifunctional DC electric springs for improving voltage quality of DC grids," *IEEE Tran. Smart Grid*, vol. PP, no. 99, pp. 1−1, Sep. 2016.
[11] C. K. Lee, N. R. Chaudhuri, B. Chaudhuri, and S. Y. R. Hui, "Droop control of distributed electric springs for stabilizing future power grid," *IEEE Trans. Smart Grid*, vol. 4, no. 3, pp. 1558−1566, Sep. 2013.
[12] N. Chaudhuri, C. Lee, B. Chaudhuri, and S. Hui, "Dynamic modeling of electric springs," *IEEE Trans. Smart Grid*, vol. 5, no. 5, Sep. 2013.

[13] X. Luo, Z. Akhtar, C. K. Lee, B. Chaudhuri, S. C. Tan, and S. Y. R. Hui, "Distributed voltage control with electric springs: Comparisons with STATCOM," *IEEE Trans. Smart Grid*, vol. 6, no. 1, Jan. 2015.
[14] S. C. Tan, C. K. Lee, and S. Y. R. Hui, "General steady-state analysis and control principle of electric springs with active and reactive compensations," *IEEE Trans. Pow. Elect.*, vol. 28, no. 8, Aug. 2013.
[15] K. T. Mok, S. C. Tan, and S. Y. R. Hui, "Decoupled power angle and voltage control of electric springs," *IEEE Trans. Power Electron.*, vol. 31, no. 2, pp. 1216−1229, Feb. 2016.
[16] X. Chen, Y. Hou, S. C. Tan, C. K. Lee, and S. Y. R. Hui, "Mitigating voltage and frequency fluctuation in microgrids using electric springs," *IEEE Trans. Smart Grid*, vol. 6, no. 2, pp. 508−515, Mar. 2015.
[17] C. K. Lee and S. Y. R. Hui, "Reduction of energy storage requirements in future smart grid using electric springs," *IEEE Trans. Smart Grid*, vol. 4, no. 3, pp. 1282−1288, Sep. 2013.
[18] Q. Wang, M. Cheng, Z. Chen, and Z. Wang, "Steady-state analysis of electric springs with a novel δ control," *IEEE Trans. Power Electron.*, vol. 30, no. 12, pp. 7159−7169, Dec. 2015.
[19] K. Krishnanand, S. Hasani, J. Soni, S. Panda, "Neutral current mitigation using controlled electric springs connected to microgrids within build environment," in *Proc. IEEE ECCE*, Sep. 2014, pp. 2947−2951.
[20] S. Yan, S. C. Tan, C. K. Lee, B. Chaudhuri, and S. Y. Hui, "Electric spring for reducing power imbalance in three-phase power systems," *IEEE Trans. Power Electron.*, vol. 30, no. 7, pp. 3601−3609, Aug. 2014.
[21] Y. Yang, S. C. Tan, and S. Y. R. Hui, "Voltage and frequency control of electric spring based smart loads," in *IEEE Applied Power Electron. Confer. Expo. (APEC)*, 2016, pp. 3481−3487.
[22] M. H. Wang, S. C. Tan, and S. Y. R. Hui, "Reduction of storage capacity in DC microgrids using PV-embedded series DC electric springs," in *IEEE Applied Power Electron. Confer. Expo.*, 2016, pp. 3302−3309.
[23] Q. Wang, M. Cheng, Y. Jiang et al., "DC electric springs with DC/DC converters," in *IEEE Int. Power Electron. Motion Control (IPEMC-ECCE Asia)*, 2016, pp. 3268−3273.
[24] T. Gragicevic, J. Guerrero, J. Vasquez, D. Skrlec, "Supervisory control of an adaptive-droop regulated DC microgrid with battery management capability," *IEEE Trans. Pow. Elect.*, vol. 29, no. 2, Feb. 2014.
[25] H. Kakigano, Y. Miura, and T. Ise, "Low-voltage bipolar-type DC microgrid for super high quality distribution," *IEEE Trans. Power Electron.*, vol. 25, no. 12, pp. 3066−3075, Dec. 2010.
[26] J. B. Rawlings and D. Q. Mayne, *Model Predictive Control: Theory and Design*, Nob Hill Publishing, 2009.
[27] J. Maciejowski, *Predictive Control with Constraints*, Prentice Hall, 2002.
[28] C. Li, S. Chaudhary, M. Savaghebi, J. Vasquez, and J. Guerrero, "Power flow analysis for low-voltage AC and DC microgrids considering droop control and virtual impedance," *IEEE Tran. Smart Grid*, in press.
[29] C. Li, F. Bosio, F. Chen S. K. Chaudhary, J. C. Vasquez and J. M. Guerrero, "Economic dispatch for operating cost minimization under real-time pricing in droop-controlled DC microgrids," *IEEE Trans. Emerg. Sel. Topics Power Electron.*, vol. 5, no. 1, pp. 587−595, Mar. 2017.
[30] "48 volt DC power distribution system use your renewable energy first," http://sunshineworks.com/48-volt-dc-power-distribution.htm.
[31] "Grid energy storage," U.S. Department of Energy, Dec. 2013, http://www.sandia.gov/ess/docs/other/Grid Energy Storage Dec 2013.pdf.
[32] Y. Yang, S. S. Ho, S. C. Tan, and S. Y. R. Hui, "Small-signal model and stability of electric springs in power grids," *IEEE Trans. Smart Grid*, vol. PP, no. 99, pp. 1−1, Mar. 2016.

Yun Yang (S'13) received the B.S. degree from Wuhan University, Wuhan, China, in 2012. He is currently working toward the Ph.D. degree in Power Electronics Research Group, Department of Electrical and Electronic Engineering, The University of Hong Kong, Hong Kong. His current research interests include modeling and control of power converters in smart grids, LED lighting systems, and wireless power transfer systems.

He serves as a reviewer for IEEE Transactions on Power Electronics, IEEE Transactions on Industrial Electronics, and IEEE Transactions on Smart Grid.

Siew-Chong Tan (M'06–SM'11) received the B.Eng. (Hons.) and M.Eng. degrees in electrical and computer engineering from the National University of Singapore, Singapore, in 2000 and 2002, respectively, and the Ph.D. degree in electronic and information engineering from the Hong Kong Polytechnic University, Hong Kong, in 2005.

From October 2005 to May 2012, he worked as Research Associate, Postdoctoral Fellow, Lecturer, and Assistant Professor in Department of Electronic and Information Engineering, Hong Kong Polytechnic University, Hong Kong. From January to October 2011, he was Senior Scientist in Agency for Science, Technology and Research (A*Star), Singapore. He is currently an Associate Professor in Department of Electrical and Electronic Engineering, The University of Hong Kong, Hong Kong. Dr. Tan was a Visiting Scholar at Grainger Center for Electric Machinery and Electromechanics, University of Illinois at Urbana-Champaign, Champaign, from September to October 2009, and an Invited Academic Visitor of Huazhong University of Science and Technology, Wuhan, China, in December 2011. His research interests are focused in the areas of power electronics and control, LED lightings, smart grids, and clean energy technologies.

Dr. Tan serves extensively as a reviewer for various IEEE/IET transactions and journals on power, electronics, circuits, and control engineering. He is an Associate Editor of the IEEE Transactions on Power Electronics. He is a coauthor of the book *Sliding Mode Control of Switching Power Converters: Techniques and Implementation* (Boca Raton: CRC, 2011).

Shu Yuen Ron Hui (M'87–SM'94–F'03) received his BSc (Eng) Hons at the University of Birmingham in 1984 and a D.I.C. and PhD at Imperial College London in 1987. Presently, he holds the Philip Wong Wilson Wong Chair Professorship at the University of Hong Kong and a part-time Chair Professorship at Imperial College London. He has published over 300 technical papers, including more than 220 refereed journal publications. Over 60 of his patents have been adopted by industry. He is an Associate Editor of the IEEE Transactions on Power Electronics and IEEE Transactions on Industrial Electronics, and an Editor of the IEEE Journal of Emerging and Selected Topics in Power Electronics. His inventions on wireless charging platform technology underpin key dimensions of Qi, the world's first wireless power standard, with freedom of positioning and localized charging features for wireless charging of consumer electronics. He received the IEEE Rudolf Chope R&D Award from the IEEE Industrial Electronics Society and the IET Achievement Medal (The Crompton Medal) in 2010, and IEEE William E. Newell Power Electronics Award in 2015. He is a Fellow of the Australian Academy of Technological Sciences & Engineering and the Royal Academy of Engineering, U.K.